

# ARTSY-J: Convenient and precise measurement of $^3J_{\text{HNH}\alpha}$ couplings in medium-size proteins from TROSY-HSQC spectra



Julien Roche<sup>1</sup>, Jinfa Ying<sup>1</sup>, Yang Shen, Dennis A. Torchia, Ad Bax\*

Laboratory of Chemical Physics, National Institute of Diabetes and Digestive and Kidney Diseases, National Institutes of Health, Bethesda, MD 20892, USA

## ARTICLE INFO

### Article history:

Received 12 March 2016  
Revised 22 April 2016  
Accepted 2 May 2016  
Available online 3 May 2016

### Keywords:

Backbone torsion angle  
Gly  
Karplus equation  
TROSY  
GB3  
HIV-1 Protease  
Protein NMR

## ABSTRACT

A new and convenient method, named ARTSY-J, is introduced that permits extraction of the  $^3J_{\text{HNH}\alpha}$  couplings in proteins from the relative intensities in a pair of  $^{15}\text{N}$ - $^1\text{H}$  TROSY-HSQC spectra. The pulse scheme includes  $^3J_{\text{HNH}\alpha}$  dephasing of the narrower TROSY  $^1\text{H}^{\text{N}}\{-^{15}\text{N}\}$  doublet component during a delay, integrated into the regular two-dimensional TROSY-HSQC pulse scheme, and compares the obtained intensity with a reference spectrum where  $^3J_{\text{HNH}\alpha}$  dephasing is suppressed. The effect of passive  $^1\text{H}^{\alpha}$  spin flips downscales the apparent  $^3J_{\text{HNH}\alpha}$  coupling by a uniform factor that depends approximately linearly on both the duration of the  $^3J_{\text{HNH}\alpha}$  dephasing delay and the  $^1\text{H}$ - $^1\text{H}$  cross relaxation rate. Using such a correction factor, which accounts for the effects of both inhomogeneity of the radiofrequency field and  $^1\text{H}^{\alpha}$  spin flips, agreement between prior and newly measured values for the small model protein GB3 is better than 0.3 Hz. Measurement for the HIV-1 protease homodimer (22 kDa) yields  $^3J_{\text{HNH}\alpha}$  values that agree to better than 0.7 Hz with predictions made on the basis of a previously parameterized Karplus equation. Although for Gly residues the two individual  $^3J_{\text{HNH}\alpha}$  couplings cannot be extracted from a single set of ARTSY-J spectra, the measurement provides valuable  $\phi$  angle information.

Published by Elsevier Inc.

## 1. Introduction

$^3J_{\text{HNH}\alpha}$  couplings in peptides and proteins are particularly useful parameters for defining the corresponding backbone torsion angles,  $\phi$  [1,2]. When comparing experimental  $^3J_{\text{HNH}\alpha}$  couplings with values obtained from optimized Karplus equations and X-ray derived  $\phi$  angles, a pairwise root-mean-square difference (rmsd) could be obtained that typically was at least 0.8 Hz [2–4]. Subsequent work has shown that up to twofold better agreement can be obtained when using NMR or X-ray structures that have been refined with residual dipolar couplings (RDCs). These refined structures no longer require the simplifying assumption that the hydrogens are located in idealized geometric positions [5–7].

A myriad of different experimental methods has been described in the literature for measurement of  $^3J_{\text{HNH}\alpha}$  couplings. Considering that the one-dimensional (1D) NMR spectrum of a protein is usually insufficiently resolved for measuring these couplings directly, these methods mostly relied on 2D or 3D NMR spectroscopy. Broadly speaking, the methods can be distinguished in those that obtain the  $^3J_{\text{HNH}\alpha}$  couplings from either the difference in frequency

of the 2D or 3D multiplet components, or from so-called quantitative- $J$  measurements, where the coupling value is obtained from the relative intensity of resonances. Examples of the first group include addition and subtraction of in-phase and anti-phase  $^1\text{H}^{\text{N}}\{-^1\text{H}^{\alpha}\}$  doublets in NOESY and COSY spectra [3], E.COSY measurements [8–10],  $J$ -resolved methods [11–13], multiple quantum methods that eliminate the effect of fast relaxation of the passive spin [14,5], or simply the measurement of antiphase splittings in resolution-enhanced COSY spectra. Very recently, we demonstrated that for small or disordered proteins, the favorable  $^1\text{H}^{\text{N}}$  relaxation properties in TROSY-HSQC spectra [15] permit direct measurement of the in-phase  $^3J_{\text{HNH}\alpha}$  splittings, provided that some precautions are taken [16]. Examples of intensity-based measurements, can be subdivided into methods where the transfer of  $\text{H}^{\text{N}}$  to  $\text{H}^{\alpha}$  or  $\text{H}^{\alpha}$  to  $\text{H}^{\text{N}}$  is quantified from the ratio of the  $^1\text{H}$ - $^1\text{H}$  diagonal and cross peak intensities, including the HNHA [4] and the related HA[HB,HN](CACO)NH experiments [17], and those where the intensity decay of the amide  $^1\text{H}^{\text{N}}$  signal resulting from  $^3J_{\text{HNH}\alpha}$  dephasing is fitted [18,19].

Here, we describe a new method that is most closely related to this last group of experiments, but that compares the intensities of signals that are and that are not subject to  $^3J_{\text{HNH}\alpha}$  dephasing. During the requisite dephasing delay, which now can be considerably shorter than  $0.5/{}^3J_{\text{HNH}\alpha}$ , favorable TROSY relaxation interference between the  $^1\text{H}^{\text{N}}$  CSA and the  $^1\text{H}^{\text{N}}\text{-}^{15}\text{N}$  dipolar coupling [15]

\* Corresponding author.

E-mail address: [bax@nih.gov](mailto:bax@nih.gov) (A. Bax).

<sup>1</sup> These authors contributed equally.

further minimizes transverse relaxation losses and makes the experiment applicable to medium size (10–30 kDa) proteins. It should be noted that for maximum benefit of the TROSY line-narrowing effect in proteins, the method is often combined with perdeuteration followed by back-exchange of the amide protons. For measurement of  ${}^3J_{\text{HNH}\alpha}$ , such perdeuteration is clearly not an option, and attainable line widths are broader than if TROSY detection is combined with perdeuteration.

Although, in particular for larger proteins, backbone torsion angle restraints are nowadays most commonly derived from chemical shift analysis, we note that chemical shifts depend on both  $\phi$  and  $\psi$  torsion angles, and to a smaller but non-negligible extent on a range of other factors, incl. H-bonding, sidechain torsion angles, and electric fields from nearby charged atoms [20–22]. This results in considerable uncertainty in the predicted  $\phi$  value, and a (typically small) fraction of residues for which no reliable prediction can be made.  ${}^3J_{\text{HNH}\alpha}$  values are solely dominated by  $\phi$ , and therefore remain a valuable source of precise structural information.

## 2. Experimental section

The reference and attenuated ARTSY-J spectra were recorded for 1.2-mM  ${}^{15}\text{N}$ -enriched GB3 (20 mM sodium phosphate buffer, 50 mM NaCl, pH 6.5, and 0.05% sodium azide) at 293 K in an interleaved manner on a 800 MHz Bruker Avance III spectrometer running Topspin 3.1, equipped with a z-axis gradient cryogenic TCI probe. Each experiment consists of  $1024^* (F_2, {}^1\text{H}, 98.3 \text{ ms}) \times 300^* (F_1, {}^{15}\text{N}, 108 \text{ ms})$  complex data points. Spectra were recorded for several durations of the total dephasing time, ranging from 28 to 50 ms. With an interscan delay of 1.2 s and 8 scans per FID, the total recording time was 4 h for each pair of spectra. For data processing, the detected dimension was apodized using 25-Hz exponential line broadening in the  ${}^1\text{H}$  dimension. A truncated cosine window (corresponding to a cosine function running from  $0^\circ$  to  $86^\circ$ ) was applied to apodize the  ${}^{15}\text{N}$  dimension. The time domain data were zero filled prior to Fourier transformation, to yield a final data matrix size of  $4096 (F_2, {}^1\text{H}) \times 2048 (F_1, {}^{15}\text{N})$  real points. All spectra were processed and analyzed using the NMRPipe software package [23].

The interleaved spectra for the HIV-1 protease sample (150  $\mu\text{M}$  dimer; pH 5.7, 20 mM sodium phosphate) were recorded at 298 K on a 900 MHz Bruker Avance III, equipped with a z-axis gradient cryogenic TCI probe. The interleaved time domain data matrix consists of  $2 \times 1280^* (F_2, {}^1\text{H}, 97.3 \text{ ms}) \times 175^* (F_1, {}^{15}\text{N}, 54.3 \text{ ms})$  complex data points, and was processed in the same way as described above for GB3. The total dephasing time was set to 30 ms. With an interscan delay of 1.2 s and 64 scans per FID, the total recording time for the two interleaved spectra was approximately 17 h. To estimate the  ${}^1\text{H}$  TROSY  $T_2$ , a reference experiment with a 12-ms dephasing time was performed with 16 scans per FID and otherwise identical acquisition parameters. The intensity ratio of the two reference spectra with different dephasing times was scaled to reflect the total number of scans before extracting the  $T_2$  values.

## 3. Results and discussion

### 3.1. Description of the pulse scheme

The pulse scheme for the new method is sketched in Fig. 1. The scheme is very similar to the ARTSY experiment, originally introduced to measure  ${}^1J_{\text{NH}}$  splittings, and particularly useful for measurement of  ${}^1D_{\text{NH}}$  residual dipolar couplings (RDCs) in medium size proteins [24]. The new pulse sequence, named ARTSY-J, is

again very similar to the regular TROSY-HSQC experiment. However, rather than an INEPT transfer of  ${}^1\text{H}^{\text{N}}$  magnetization to  ${}^{15}\text{N}$ , ARTSY-J uses an ST2PT pulse sequence element [25,26] to transfer magnetization from the upfield  ${}^1\text{H}^{\text{N}}\{-{}^{15}\text{N}\}$  doublet component to the downfield  ${}^{15}\text{N}$  doublet component (between time points c and g in Fig. 1). The ST2PT element is preceded by an INEPT magnetization transfer step (between time points a and b) to convert Boltzmann  ${}^{15}\text{N}$  magnetization,  $N_z$ , into  $2H_zN_z$ , where the phase ( $-y$ ) of the  ${}^{15}\text{N}$  pulse at time point b is chosen such that this term enhances the upfield  ${}^1\text{H}^{\text{N}}\{-{}^{15}\text{N}\}$  doublet component. During the  $c$ - $f$  time interval of the subsequent ST2PT transfer, two band-selective IBURP2-shaped [27]  ${}^1\text{H}^\alpha$  pulses are applied either at positions shown in scheme A (Experiment A) or B (Experiment B; Fig. 1). In experiment B,  $J_{\text{HNH}\alpha}$  dephasing is effective for the full duration from c to f, minus the durations of the two IBURP2 pulses:  $\tau_d = 2A_3 + 2\delta = 2A_1 + 2A_2 + 2\delta$ , where  $A_1$ ,  $A_2$ ,  $A_3$  and  $\delta$  are defined in Fig. 1. Instead, if the IBURP2 pulses are applied at positions marked in scheme A,  $J_{\text{HNH}\alpha}$  dephasing is active for a time  $2A_1 - 2A_2 + 2\delta$ . By setting  $A_2 = A_1 + \delta$ , no net  $J_{\text{HNH}\alpha}$  dephasing takes place in experiment A.

Ignoring  ${}^1\text{H}^\alpha$  or  ${}^1\text{H}^{\text{N}}$  spin relaxation during the interval between time points c and f,  $J_{\text{HNH}\alpha}$  dephasing in experiment B converts the upfield  ${}^1\text{H}\{-{}^{15}\text{N}\}$  doublet component,  $I_y - 2I_yN_z$ , into  $(I_y - 2I_yN_z)\cos(\pi J_{\text{HNH}\alpha}\tau_d) - 2(I_xH_z^2 - 2I_xH_z^2N_z)\sin(\pi J_{\text{HNH}\alpha}\tau_d)$ . Only the first of these two terms is transferred to  ${}^{15}\text{N}$  TROSY transverse magnetization at time point g, yielding  $(N_x + 2I_zN_x)\cos(\pi J_{\text{HNH}\alpha}\tau_d)$ . The second term is converted into higher order product terms by the  $90^\circ_y$   ${}^1\text{H}$  pulse at time f, which are eliminated by the subsequent gradients as well as the band-selective pulses applied during the final ST2PT transfer (between time points i and j). Following gradient encoding of the transverse  ${}^{15}\text{N}$  magnetization by gradients  $G_7$  and  $G_8$  in the standard manner [28], and evolution for a duration  $t_1$ , with an optional hard-pulse/band-selective pulse at time point h to remove long range  ${}^1\text{H}\{-{}^{15}\text{N}\}$  J couplings in the  $t_1$  dimension [29,16],  ${}^{15}\text{N}$  magnetization is transferred back in the standard manner to  ${}^1\text{H}^{\text{N}}$  for TROSY detection [25,26]. The final result is a regular  ${}^1\text{H}\{-{}^{15}\text{N}\}$  TROSY-HSQC spectrum, but the intensity obtained in experiment B is scaled by  $\cos(\pi J_{\text{HNH}\alpha}\tau_d)$  relative to that in experiment A. To a first approximation,  ${}^3J_{\text{HNH}\alpha}$  is then simply derived from

$${}^3J_{\text{HNH}\alpha} = \cos^{-1}(I_B/I_A)/(\pi\tau_d) \quad (1)$$

where  $I_B$  and  $I_A$  are the intensities for any given amide correlation in the respective TROSY-HSQC spectra.

### 3.2. Precision of the $J_{\text{HNH}\alpha}$ measurement

The precision at which  ${}^3J_{\text{HNH}\alpha}$  can be extracted from the data depends on the experimental uncertainty in the ratio,  $Q = I_B/I_A$ . If equal numbers of scans are recorded for the reference (A) and attenuated (B) spectrum, the uncertainty in  $Q$  can be derived by assuming identical Gaussian noise of root-mean-square (rms) amplitude,  $N$ , in both the reference and attenuated spectra. Since  $Q$  is the ratio of two independent measurements, error propagation for division yields the uncertainty  $\sigma_Q$  in the value of  $Q$ :

$$\sigma_Q = \left| \frac{I_B}{I_A} \right| \sqrt{\left( \frac{N}{I_A} \right)^2 + \left( \frac{N}{I_B} \right)^2} = (N/I_A) \sqrt{Q^2 + 1} \quad (2)$$

where  $N/I_A$  represents the inverse signal to noise ratio (S/N) in the reference spectrum. In practice, the dephasing delay  $\tau_d$  is chosen to yield  $Q$  values in the 0.5–1 range, meaning that the uncertainty in  $Q$  is 1.1–1.4 times higher than the inverse of the signal-to-noise ratio in the reference spectrum. The uncertainty,  $\varepsilon$ , in  ${}^3J_{\text{HNH}\alpha}$  extracted from Eq. (1) is then given by

$$\varepsilon = \sigma_Q / [\pi\tau_d \sin(\pi J_{\text{HNH}\alpha}\tau_d)] \quad (3)$$

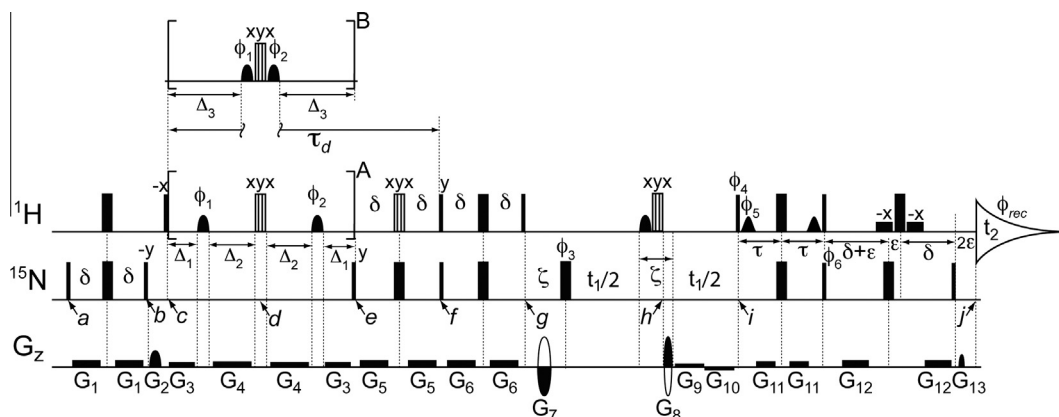


**Fig. 1.** Pulse scheme of the ARTSY-J experiment. The pulse scheme is executed twice, once (A) as shown (reference spectrum) and once (B) with element B substituting for element A. The total  ${}^3J_{\text{HNH}\alpha}$  dephasing time in B equals  $\tau_d = 2\Delta_3 + 2\delta$ , where  $\Delta_3 = \Delta_1 + \Delta_2$ , and  $\Delta_1 = \Delta_2 - \delta$ . Therefore,  $\tau_d$  equals the total duration between time points c and f, minus the shaped  ${}^1\text{H}$  pulses. Pulses prior to point b serve to transfer  ${}^{15}\text{N}$  Boltzmann magnetization to  ${}^1\text{H}$ . The element between time points c and f is a ST2PT element that transfers magnetization from the TROSY  ${}^1\text{H}^{\alpha}\text{-}({}^{15}\text{N})$  doublet component to the TROSY  ${}^{15}\text{N}\text{-}({}^1\text{H}^{\alpha})$  component. Shaped  ${}^1\text{H}$  pulses with phases  $\phi_1$  and  $\phi_2$  are of the IBURP2 type [27], centered near the  $\text{H}_2\text{O}$  frequency at 4.57 ppm and aimed to invert the  ${}^1\text{H}^{\alpha}$  magnetization (2.0 ms duration for  $>90\%$   ${}^1\text{H}^{\alpha}$  inversion over a  $\pm 1.3$  ppm bandwidth at 800 MHz). The shaped/composite  $180^\circ$  pulse combination, just prior to time point h, is optional and can be beneficial for smaller proteins if very high  ${}^{15}\text{N}$  resolution is required. This combination of an IBURP2 pulse (1.1-ms duration at 800 MHz, centered at 8.7 ppm) and a non-selective, composite pulse serves to invert all but  ${}^1\text{H}^{\alpha}$  at the midpoint of  $t_1$  evolution, effectively removing long range couplings to  ${}^{15}\text{N}$ . Other shaped  ${}^1\text{H}$  elements are regular water-flip-back pulses, as used in the original ST2PT scheme [25]. Narrow and wide filled bars represent non-selective  $90^\circ$  and  $180^\circ$  pulses, while the vertically hatched open bars represent  $90^\circ_x\text{-}234^\circ_y\text{-}90^\circ_x$  composite  $180^\circ$   ${}^1\text{H}$  inversion pulses. The filled rectangular boxes surrounding the last  $180^\circ$   ${}^1\text{H}$  pulse correspond to 1-ms rectangular pulses at the  $\text{H}_2\text{O}$  frequency that in combination function as a WATERGATE element [47]. All pulses are applied along x unless otherwise indicated. Durations of all shaped pulses are for a  ${}^1\text{H}$  frequency of 800 MHz and should be scaled inversely relative to this frequency if applied at higher or lower magnetic fields. Delay durations:  $\delta = 2.66$  ms;  $\epsilon = 235$   $\mu\text{s}$ ;  $\zeta = 2.35$  ms  $\mu\text{s}$ ;  $\tau \approx 2.3$  ms (somewhat shorter than  $1/(4J_{\text{HNH}\alpha})$  to minimize the  ${}^{15}\text{N}$  anti-TROSY component [26]). Phase cycling:  $\phi_1 = x, x, -x, -x$ ;  $\phi_2 = 4x, 4(-x)$ ;  $\phi_3 = x, y$ ;  $\phi_4 = y$ ;  $\phi_5 = y$  (or  $-y$  if the band-selective decoupling element at time h is not used)  $\phi_6 = y$ ;  $\phi_{\text{rec}} = x, -x$ . To obtain the second FID for the echo-antiecho quadrature detection, the  $\phi_4, \phi_5$ , and  $\phi_6$  phases together with encoding gradients  $G_7$  and  $G_8$  need to be inverted in the regular manner [28]. Gradients are sine-bell or rectangular shaped, as marked in the figure, with durations:  $G_{1,2,3,4,5,6,7,8,9,10,11,12,13} = 2.46, 0.47, 0.711, 0.78, 2.46, 2.46, 1.05, 0.95, t_1/4, t_1/4, 0.787, 1.35, \text{ and } 0.207$  ms, and strengths of 1.33, 28.7,  $-8.4, -1.4, 4.9, 13.3, -25.9, 25.9, 0.91, -0.91, 2.1, -32.9$ , and 25.9 G/cm. Note that the duration of decoding pulse  $G_{13}$  is empirically optimized to yield maximum signal, and can differ from its theoretical value,  $|\gamma_{\text{N}}/\gamma_{\text{H}}|(|G_7| + |G_8|)$ , by several microseconds due to rise and fall times of short gradient pulses.

Note that the signal to noise ratio, and thereby  $1/\sigma_{\text{O}}$ , scales with  $\exp(-\tau_d/T_2)$ , where  $T_2$  is the transverse relaxation time of the TROSY  ${}^1\text{H}\text{-}{}^{15}\text{N}$  doublet component. In the limit where  $T_2 \ll 1/J_{\text{HNH}\alpha}$ ,  $\epsilon$  is minimized for  $\tau_d \approx 2T_2$ . In practice, a somewhat shorter  $\tau_d$  may be chosen to reduce the effect of  ${}^1\text{H}\text{-}{}^1\text{H}$  cross relaxation which, as discussed below, can lead to an underestimate of the true  $J_{\text{HNH}\alpha}$  value [30,19]. We prefer to use  $\tau_d$  values in the 30–50 ms range for proteins with rotational correlation times in the 15–5 ns range, for which the ARTSY-J experiment appears the method of choice in our hands. The uncertainty in the extracted  $J_{\text{HNH}\alpha}$  value scales approximately inversely with its size, but assuming a typical S/N ratio of 50:1 in the reference spectrum the precision of the measurement remains more than adequate for all but the smallest couplings (Fig. 2). Even though the spectral S/N, and thereby the extracted precision of  $J_{\text{HNH}\alpha}$ , is adversely impacted by factors that increase  ${}^1\text{H}^{\alpha}$  transverse relaxation, e.g. solvent exchange, conformational exchange, or external relaxation agents, they attenuate the reference and dephased spectra by the same factor, and to a very good approximation do not cause any systematic error in the extracted coupling value.

### 3.3. Systematic errors from pulse imperfections

In practice, the  $I_A(\tau_d)/I_B(\tau_d)$  intensity ratio can also be affected by systematic errors, and the pulse scheme therefore has been designed to keep such errors at a minimum. First, schemes A and B have been constructed such as to contain the same number and types of pulses, such that effects of imperfections of these pulses to first order cancel when considering the ratio of  $I_A$  and  $I_B$ . Second, the non-selective  $180^\circ$  refocusing pulses applied during the  ${}^3J_{\text{HNH}\alpha}$  dephasing period are of the  $90^\circ_x\text{-}234^\circ_y\text{-}90^\circ_x$  type, such as to be minimally sensitive to both radiofrequency inhomogeneity and offset effects [31]. Whereas incomplete inversion of the  ${}^1\text{H}^{\alpha}$

spin by either of these pulses simply attenuates the observed magnetization by equal fractions in schemes A and B, incomplete inversion of  ${}^1\text{H}^{\alpha}$  in scheme B makes dephasing of the  ${}^3J_{\text{HNH}\alpha}$  evolution incomplete at time point f, where it is effectively transferred to  ${}^{15}\text{N}$ , thereby artificially raising the intensity of  $I_B$ . On the other hand, incomplete  ${}^1\text{H}^{\alpha}$  inversion by the two composite pulses in scheme A will interfere with the rephasing of the  ${}^3J_{\text{HNH}\alpha}$  evolution, causing the reference intensity to be too low. The net effect is a small, systematic underestimate in the  ${}^3J_{\text{HNH}\alpha}$  value obtained from Eq. (1) by an amount that scales approximately linearly with the size of the coupling.

Incomplete  ${}^1\text{H}^{\alpha}$  spin inversion by the band-selective IBURP2 pulses has the same effect as mentioned above for the non-selective pulses: incomplete dephasing for scheme B and incomplete rephasing for scheme A, again resulting in systematically too high an  $I_B/I_A$  ratio, or systematically too small a value for  ${}^3J_{\text{HNH}\alpha}$  extracted using Eq. (1). Unlike for the non-selective  $180^\circ$  pulses, the band-selective pulses are not readily compensated for inhomogeneity of the radiofrequency field without considerably lengthening their minimal duration. The latter solution would result in sensitivity loss, and we therefore prefer to simply correct the ratio by using an empirical correction factor (see below).

### 3.4. Systematic errors from ${}^1\text{H}\text{-}{}^1\text{H}$ cross relaxation

A more insidious type of systematic error is caused by the presence of  ${}^1\text{H}^{\alpha}$  spin flips during the dephasing time  $\tau_d$  [30,4,19]. These spin flips affect the signal intensities of both the reference and attenuated spectra, but to different extents. Their effect on  ${}^3J_{\text{HNH}\alpha}$  measurements was simulated by using Goldman's equation [32] to calculate the evolution of the expectation values of in-phase ( $I_y$ ) and antiphase ( $2I_xS_z$ ) magnetization ( $I = \text{H}^{\text{N}}, S = \text{H}^{\alpha}$ ) [4,19]:

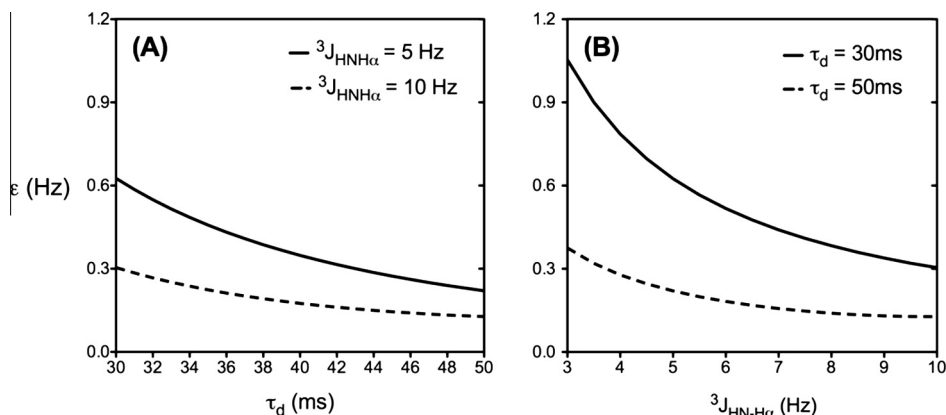


**Fig. 2.** Random uncertainty,  $\epsilon$ , in the extracted  $J_{\text{HNH}\alpha}$  value. (A) Dependence of  $\epsilon$  on the duration of  $\tau_d$ , for  $J_{\text{HNH}\alpha}$  values of 5 Hz (solid line) and 10 Hz (dashed line) assuming a  $S/N = 50$  in the reference spectrum. (B) Dependence of  $\epsilon$  on the size of  $J_{\text{HNH}\alpha}$  assuming a  $S/N = 50$  in the reference spectrum and  $\tau_d = 30$  ms (solid line) or 50 ms (dashed line).

$$dM/dt = -RM(t)$$

where,

$$M = \begin{bmatrix} I_y \\ 2I_x S_z \end{bmatrix}, \quad R = \begin{bmatrix} R_2 & \pi J \\ -\pi J & R_2 + R_{1\alpha} \end{bmatrix} \quad (4)$$

In this equation, the cross relaxation of the  ${}^1\text{H}^\alpha$  spins is accounted for by the inclusion of the “single-spin” relaxation rate,  $R_{1\alpha}$ , in the rate matrix  $R$ ,  $R_2$  is the  $\text{H}^N$  transverse relaxation rate, and  $J$  is  ${}^3J_{\text{HNH}\alpha}$ . The formal solution of this equation is [33]:

$$M(t) = e^{-Rt}M(0) = A(t)M(0) \quad (5)$$

The elements of the  $2 \times 2$  matrix  $A(t)$  are provided in the Supporting Information, and the  $M(0)$  vector is composed of the values of  $I_y$  and  $2I_x S_z$  at the beginning of the dephasing period. Considering that the  ${}^1\text{H}^N$ - $[{}^1\text{H}^\alpha]$  de- or re-phasing process is not impacted by the non-selective (composite)  ${}^1\text{H}$   $180^\circ$  pulses, their presence will be ignored in the discussion below. Then, if the total duration of the  $J$ -dephasing and rephasing period equals  $\tau_d = \tau_1 + \tau_2$ , with  $\tau_1 = 2\Delta_1$ , and  $\tau_2 = 2\Delta_1 + 4\delta$ , and refocusing pulses are applied to the  $S$ -spins in the middle of these  $\tau_1$  and  $\tau_2$  periods,  $M(\tau_d)$  is given by

$$M(\tau_d) = A(\tau_2/2)EA((\tau_1 + \tau_2)/2)EA(\tau_1/2)M(0) \quad (6)$$

where,

$$E = \begin{bmatrix} 1 & 0 \\ 0 & -1 \end{bmatrix}$$

The matrix  $E$  simulates the effect of the refocusing pulses by inverting the sign of  $2I_x S_z$  in the middle of the  $\tau_1$  and  $\tau_2$  periods. As noted earlier, when  $R_{1\alpha}$  is not small,  $J$  calculated from Eq. (1) is in error and  $J$  obtained using this equation below will be referred to as the apparent  $J$ ,  $J_{\text{app}}$ . Numerical simulations using Eq. (6) show that to an excellent approximation, the true  $J$  value can be obtained from  $J_{\text{true}} = cJ_{\text{app}}$  where  $c$  is simply a scale factor that depends on the product  $R_{1\alpha} \tau_d$ , but is independent of  $J_{\text{true}}$ . This is shown in Fig. 3A, which displays plots of  $J_{\text{app}}$  vs.  $J_{\text{true}}$ , for  $R_{1\alpha} \tau_d$  from 0 to 2.4. If an estimate of  $R_{1\alpha}$  is available from relaxation experiments or from protein structural information, then the measured intensity ratio  $I_B/I_A$  can be used together with the parameters of the pulse sequence to obtain the correct value  ${}^3J_{\text{HNH}\alpha}$ . More simply, for nearly all practical applications,  $J_{\text{app}}$ , together with the following simple empirical formula provides an accurate estimate of  ${}^3J_{\text{HNH}\alpha}$ .

$${}^3J_{\text{HNH}\alpha} \cong cJ_{\text{app}}$$

where the scale factor  $c$  depends only upon  $R_{1\alpha} \tau_d$  and is given by,

$$c = (1 + 0.206R_{1\alpha} \tau_d) \quad (7)$$

Note that, in the macromolecular limit

$$R_{1\alpha} = (\mu_0/40\pi) \tau_c \hbar^2 \gamma_H^4 \sum_{i=1}^n r_{\alpha i}^{-6} \quad (8)$$

depends linearly on the rotational correlation time,  $\tau_c$ , and on the number of local protons  $i = 1 \dots n$  whose distance from  $\text{H}^\alpha$ ,  $r_{\alpha i}$  is  $< \sim 5$  Å. Replacing all such protons by a pseudo-spin at a distance  $\{\sum_i r_{\alpha i}^{-6}\}^{-1/6} \approx 1.84$  Å from  $\text{H}^\alpha$ , yields  $R_{1\alpha} \approx 1.47 [\tau_c/(1 \text{ ns})] \text{ s}^{-1}$ . This latter relation offers a semi-quantitative estimate of what scale factor to expect for a given protein.

The blue line in Fig. 3B compares apparent  $J$  couplings with their true values for the case where  $R_{1\alpha} = 60 \text{ s}^{-1}$  (corresponding to a large protein with  $\tau_c \approx 40$  ns) and  $\tau_d = 30$  ms. Scaling of these values by  $c = 1.37$  (see Eq. (7)) then yields values (green line) that fall very close to the true couplings (red line). Calculations show that use of Eq. (7) scale factors results in errors of less than 2% for all values of  $J_{\text{true}} \leq 10$  Hz and  $R_{1\alpha} \tau_d < 1.2$ . Additional calculations show that scale factors obtained from Eq. (7) also have errors of less than 2% for  $R_{1\alpha} \tau_d < 1.8$ , provided that  $\tau_2/\tau_1$  lies in the range 0.4–2.5. Note that the use of a simple scale factor to account for the effect of  $\text{H}^\alpha$  spin flips is fully compatible with the above mentioned analogous scale factor that accounts for incomplete  $\text{H}^\alpha$  inversion by the IBURP pulses applied during  $\tau_d$ , and simply requires that a  $c$  value somewhat larger than expected based on Eq. (7) be used.

### 3.5. Application to Gly residues

Measurement of  ${}^3J_{\text{HNH}\alpha}$  couplings in Gly residues has received relatively little attention to date, even though this residue type often suffers from a dearth of structural restraints. Intensity observed in the attenuated, dephased ARTSY-J spectrum is modulated by both the  ${}^3J_{\text{HNH}\alpha 2}$  and  ${}^3J_{\text{HNH}\alpha 3}$  couplings and, for a weakly coupled system, the intensity ratio relative to the reference spectrum is given by:

$$I_B/I_A = \cos(\pi^3 J_{\text{HNH}\alpha 2} \tau_d) \cos(\pi^3 J_{\text{HNH}\alpha 3} \tau_d) \quad (9)$$

Although it is not possible to extract both  ${}^3J_{\text{HNH}\alpha}$  values from a single  $I_B/I_A$  measurement, the intensity ratio provides tight restraints on the  $\phi$  angle, assuming that the Karplus curve, previously derived for non-Gly residues, is applicable to Gly residues too. Fig. 4A shows the expected  $I_B/I_A$  intensity ratio as a function of  $\phi$  for four values of the dephasing delay,  $\tau_d$ . Highest values for the ratio are expected for  $\phi$  values close to 0 or  $\pi$ , and smallest ratios are expected for  $\phi = \pm 120^\circ$ , where either  ${}^3J_{\text{HNH}\alpha 2}$  ( $\phi = +120^\circ$ ) or  ${}^3J_{\text{HNH}\alpha 3}$  ( $\phi = -120^\circ$ ) corresponds to a trans coupling.

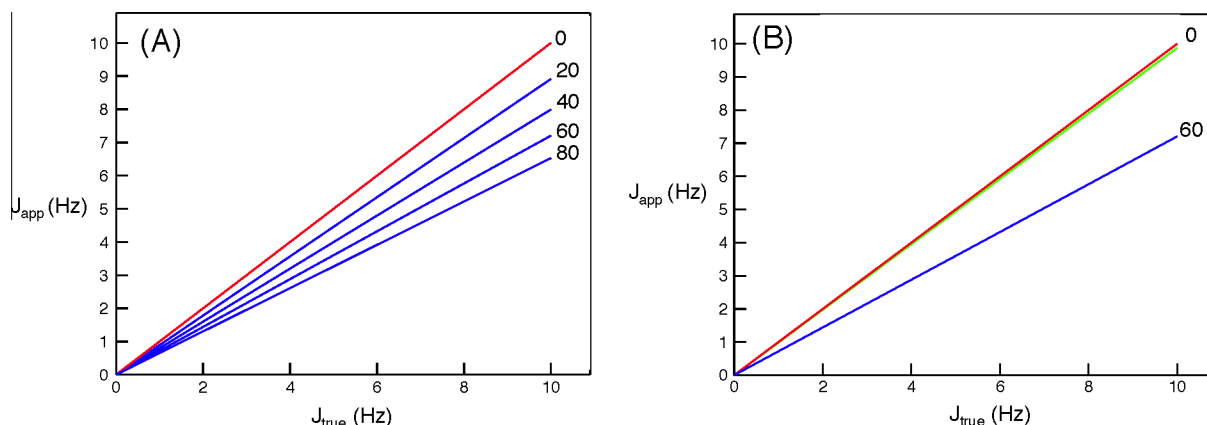


**Fig. 3.** Effect of  $^1\text{H}$ - $^1\text{H}$  cross relaxation on the  $J_{\text{HNH}\alpha}$  value extracted from the  $I_B/I_A$  ratio. (A) Plot of the apparent  $J_{\text{HNH}\alpha}$  value extracted from Eq. (1),  $J_{\text{app}}$ , versus the true  $J_{\text{HNH}\alpha}$  coupling for different values of  $R_{1\alpha}$ , marked in units of  $\text{s}^{-1}$  in the panel, and  $\tau_d = 30$  ms, using numerical calculations based on Eq. (6). (B) A linear scaling of  $J_{\text{app}}$  (blue line, for the case of  $\tau_d = 30$  ms,  $R_{1\alpha} = 60 \text{ s}^{-1}$ ) by  $c = 1 + 0.206R_{1\alpha} \tau_d$  yields a corrected  $J$  value (green) that falls very close to the true  $J_{\text{HNH}\alpha}$  (red).

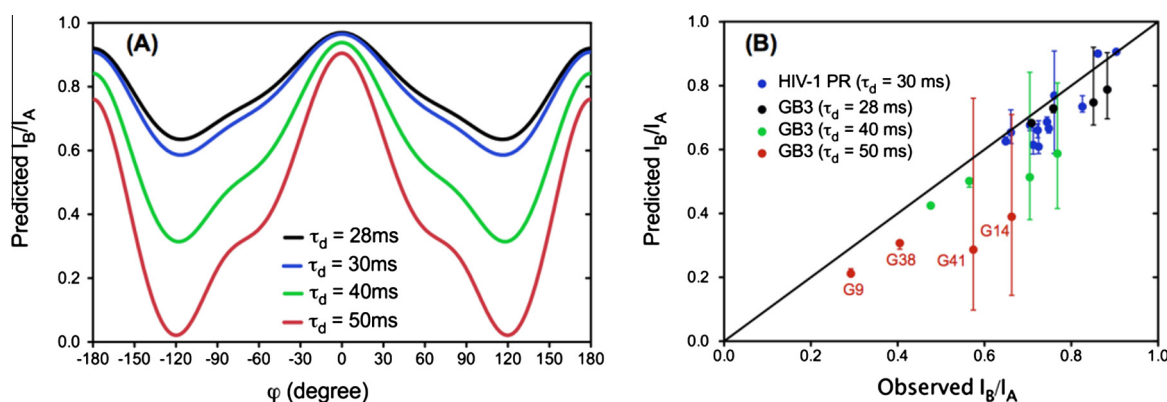


**Fig. 4.** Predicted intensity ratios for Gly residues, ignoring cross relaxation. (A) intensity ratio as a function of the backbone torsion angle  $\phi$  for different durations of the total dephasing delay,  $\tau_d$ . (B) Predicted intensity ratios versus those observed for 12 Gly residues in HIV-1 protease (blue symbols;  $\tau_d = 30$  ms) and 4 Gly residues in GB3 ( $\tau_d = 30$  ms, black; 40 ms, green; 50 ms, red). The range of ratios predicted for six high-resolution ( $\leq 1.3 \text{ \AA}$ ) X-ray structures of HIV-1 protease or two high-resolution ( $\leq 1.1 \text{ \AA}$ ) X-ray structures and two RDC-refined NMR structures (PDB entries 2OED and 2N7J) of GB3 are marked by the error bars, with the symbols corresponding to the ratios calculated for the average of the  $\phi$  angles.

In practice, strong coupling between the  $\text{H}^{\alpha 2}$  and  $\text{H}^{\alpha 3}$  protons can yield a modulation pattern more complex than Eq. (9), and the two center lines of the  $\text{H}^{\text{N}}$  doublet of doublets then will split into four components with different intensities, whereas the intensities and positions of the outer lines remain unperturbed [34]. The net result is that the modulation pattern of Eq. (9), which is dominated by the outer multiplet components, is not visibly impacted by strong coupling between the  $\text{H}^{\alpha}$  protons for  $\tau_d \leq \sim 50$  ms, permitting the same analysis as for the weak coupling case.

Accounting quantitatively for the effect of  $^1\text{H}$ - $^1\text{H}$  cross relaxation, in practice, is somewhat more involved for Gly than for other residue types. Cross relaxation involves the short ( $\sim 1.75 \text{ \AA}$ ) distance between the geminal  $\text{H}^{\alpha}$  protons, but this rate to a good approximation is only applicable for the inner components of the  $\text{H}^{\text{N}}\{-\text{H}^{\alpha}\}$  doublet of doublets. Cross relaxation impacting the outer  $\text{H}^{\text{N}}\{-\text{H}^{\alpha}\}$  components is strongly dependent on backbone conformation, and on whether the protons are solvent-exposed or packed in the interior. Nevertheless, just as is the case for the other residue types, it is clear that both cross-relaxation and imperfection of the  $180^\circ$  IBURP pulses will skew the  $I_B/I_A$  ratio toward unity from the value predicted by Eq. (9). Experimental validation will be presented below for the 16 Gly residues in the two proteins evaluated in our study.

### 3.6. Results for GB3

Fig. 5A compares the  $^3J_{\text{HNH}\alpha}$  couplings measured with the new ARTSY-J method, using  $\tau_d = 40$  ms, for the small model protein GB3 with values recently obtained by simply measuring the  $^1\text{H}$ - $^1\text{H}$  splitting in the  $^1\text{H}$  dimension of a resolution-enhanced  $^1\text{H}$ - $^{15}\text{N}$  TROSY-HSQC spectrum, recorded with precautions to prevent  $^3J_{\text{HNH}\alpha}$  dephasing during its ST2PT transfer from  $^{15}\text{N}$  to  $^1\text{H}$  [16]. With a pairwise root-mean-square difference (rmsd) of 0.29 Hz and a Pearson's correlation coefficient of  $R^2 = 0.99$ , the two sets of couplings are clearly in excellent agreement. Nevertheless, a small systematic underestimate is seen for the new values relative to those from the direct measurement, in particular for  $^3J_{\text{HNH}\alpha}$  values  $\geq \sim 7$  Hz, and increased scatter is observed for the smallest couplings. The small systematic underestimate is due in part to the above mentioned effect of imperfection of the  $180^\circ$  IBURP pulses, which causes all newly measured couplings to be slightly too small by the same factor. Larger scatter for the smallest values can be attributed to two effects: first, the noise-related uncertainty in the newly measured values scales approximately inversely with the size of the couplings and therefore is largest for the smallest couplings (Fig. 2). Second, measurement of splittings from partially overlapping doublet components in the recent

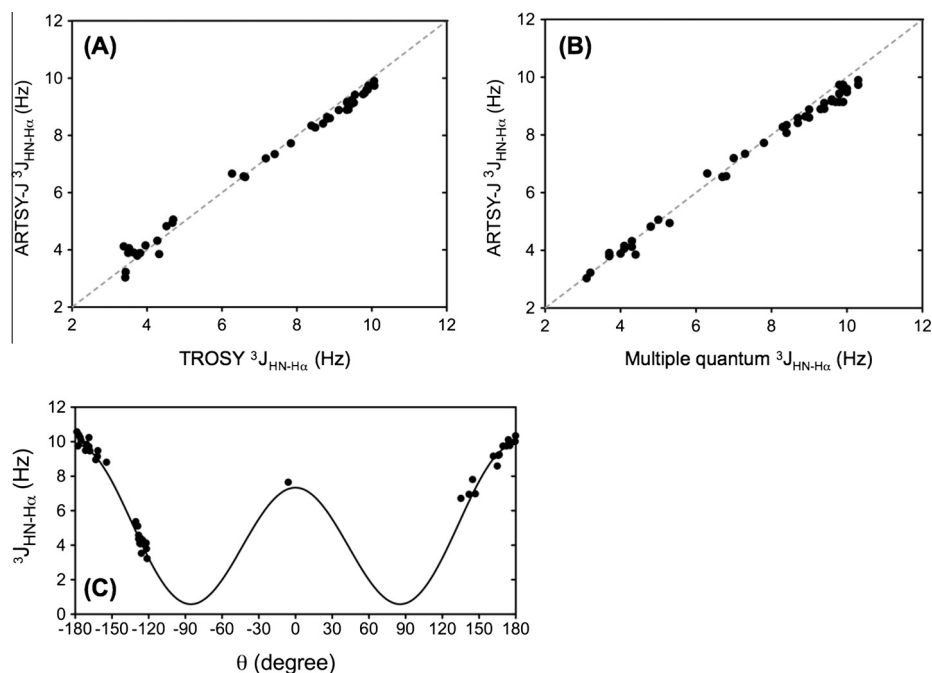


**Fig. 5.** Comparison of  $J_{\text{HNH}\alpha}$  values with previous measurements for GB3. (A) Plot of the raw (unscaled) values newly measured with the ARTSY-J method ( $\tau_d = 40$  ms; 800 MHz) with those recently measured from simple peak picking of a highly  $^1\text{H}$ -resolved TROSY-HSQC spectrum [16]. (B) Plot of the newly measured raw  $J_{\text{HNH}\alpha}$  values against those of the multiple-quantum method, that is essentially free of  $^1\text{H}$ - $^1\text{H}$  cross relaxation contamination [5]. (C) Plot of the newly measured, scaled (by a factor 1.06)  $J_{\text{HNH}\alpha}$  values as a function of the intervening H–N–C $^\alpha$ –H $^\alpha$  dihedral angle, taken from the recently refined NMR structure of GB3 (PDB entry 2N7J [39]). Relative to the previously parameterized Karplus curve [5] (solid line,  $A = 7.97$ ;  $B = -1.26$ ;  $C = 0.63$  Hz), the rmsd is 0.42 Hz.

TROSY-HSQC measurements creates larger uncertainty for the smallest couplings.

Although the rotational diffusion of GB3 is quite rapid ( $\tau_c \approx 3.34$  ns at 24 °C [35]), causing  $^1\text{H}$ - $^1\text{H}$  cross relaxation to be slow, the effect is not completely negligible. Indeed, both the prior, direct measurement of  $^3J_{\text{HNH}\alpha}$  splittings in the  $^1\text{H}$  dimension [16] and the ARTSY-J values are impacted by  $^1\text{H}$ - $^1\text{H}$  cross relaxation, but to different extents. The error introduced by cross-relaxation in the direct measurement of  $^3J_{\text{HNH}\alpha}$  in the  $^1\text{H}$  dimension of the TROSY spectrum is largest when  $^3J_{\text{HNH}\alpha}$  is small [30,19] (ca  $-0.06$  and  $-0.03$  Hz for  $J$  values of 5 and 10 Hz, respectively), whereas for the ARTSY-J experiment the error scales approximately linearly with the size of  $^3J_{\text{HNH}\alpha}$  and equals ca 3% for  $R_{1\alpha} \tau_d \approx 0.15$  (cf Eq. (7)). We therefore also compare the newly measured data to those measured with a multiple-quantum method [5], based on a concept introduced by Rexroth and Griesinger [14], which to first order are insensitive to  $^1\text{H}$ - $^1\text{H}$  cross relaxation, but somewhat less precise due to the lower sensitivity of that method. As can be seen, the newly measured data are systematically slightly smaller than those obtained from the multiple quantum method (Fig. 5B), by ca 0.55 Hz when only considering  $J$  values greater than 8 Hz, only 2% larger than the ca 4% expected based on Eq. (7). This result therefore indicates that the effect of pulse imperfection is very small (ca 2%) under the conditions that the experiment was recorded. We note, however, that without careful calibration of the IBURP2 pulses, used during the  $\tau_d$  period, this fractional error can become considerably larger.

For the smallest  $^3J_{\text{HNH}\alpha}$  values, agreement of the new data is better with the multiple-quantum measurements than with those from direct measurement of the splitting. Presumably, this observation reflects difficulties in adequately resolving the smallest splittings in the TROSY-HSQC spectrum [16], and validates the utility of the ARTSY-J method also for the accurate measurement of quite small couplings.

There are four Gly residues in GB3, with two of these (G9 and G38) located in well ordered regions of the structure, and two other residues (G14 and G41) subject to elevated backbone dynamics [35,36]. The  $\phi$  angles of G9 and G38 of two high-resolution X-ray structures (PDB entries 1IGD and 2IGD [37]) agree to within a few degrees with those of RDC-refined NMR structures (2OED [38] and 2N7J [39]), and the experimental  $I_B/I_A$  intensity ratios observed for these two residues deviates less from unity than predicted, by a factor that increases for larger  $\tau_d$  values (Fig. 4B), as expected based on Eq. (7). For G14 and G41, torsion angles span a  $35^\circ$  and  $45^\circ$  range across the four available structures, resulting in a wide range of predicted  $I_B/I_A$  intensity ratios (Fig. 4B), with the observed ratios falling closest to those in the most recent 2N7J structure [39].

### 3.7. Results for HIV-1 Protease

We also applied the ARTSY-J method to the HIV-1 protease homodimer ( $2 \times 99$  residues, 22 kDa), a protein in the size range where the  $^3J_{\text{HNH}\alpha}$  splittings cannot be resolved in a regular  $^1\text{H}$ - $^{15}\text{N}$  TROSY-HSQC spectrum. This protein has previously been studied extensively by NMR spectroscopy, both in terms of its structure and dynamic properties [40–42]. With a rotational correlation time of ca 11 ns at 25 °C [43] it represents the type of protein for which the new method is intended.

An estimate for the transverse relaxation rate of the  $^1\text{H}$  TROSY signals can be obtained by recording the reference experiment (Scheme A) of Fig. 1 for two different durations of  $\tau_d$ , yielding a substantial width for the distribution of these values:  $24.6 \pm 4.8$  ms (Fig. 6). As discussed above, in the limit of fast transverse relaxation, optimal precision for the extracted  $^3J_{\text{HNH}\alpha}$  values is obtained for a dephasing time  $\tau_d \approx 2T_2$ . However, near this optimal  $\tau_d$ , the precision is not very sensitive to its value, and a somewhat shorter-than-average  $\langle 2T_2 \rangle$  duration is used ( $\tau_d = 30$  ms),

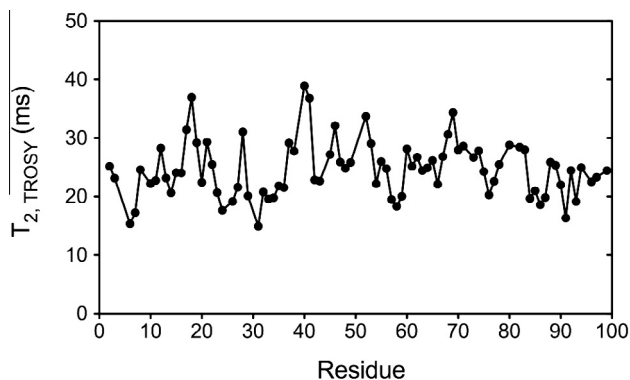


**Fig. 6.**  $^1\text{H}^{\text{N}}$  transverse relaxation times,  $T_{2,\text{TROSY}}$ , of the TROSY  $^1\text{H}$ - $^{15}\text{N}$  doublet component in HIV-1 protease, as a function of residue number. The  $T_{2,\text{TROSY}}$  values were obtained from the intensity ratio of two spectra, recorded with the reference scheme (A) of Fig. 1, using  $\tau_d$  values of 12 and 30 ms.

thereby preventing dynamic range problems that can result from large intensity differences across the spectrum (Fig. 7), while also reducing the effect of cross relaxation of the  $\text{H}^{\alpha}$  spins (Fig. 3).

Comparison of the  $I_B/I_A$  ratios derived for 68 non-Gly/Pro residues in the protease against the values of  $\cos(\pi J_{\text{HNH}\alpha} \tau_d)$ , using  $\phi$  angles taken from six X-ray structures, shows that the experimental ratios on average again fall somewhat closer to unity than predicted by the Karplus-derived  $J_{\text{HNH}\alpha}$  values (Fig. 8A). Converting the experimental ratios into  $J_{\text{HNH}\alpha}$  values shows that measured values are systematically smaller by ca 12% and use of a uniform scale factor of  $c = 1.13$  brings these values very close (rmsd 0.70 Hz) to those predicted by the Karplus curves for a set of six high-resolution ( $\leq 1.3 \text{ \AA}$ ) X-ray structures, to which hydrogens were added by MOLMOL [44]. A small improvement in the fit is obtained when refining the  $\text{H}^{\text{N}}$  positions by using recently reported RDCs [45], while keeping all other atom positions frozen (rmsd 0.64 Hz; Fig. 8B). Note that the scale factor that yields best agreement to the Karplus curve ( $c = 1.13$ ) is again slightly larger than predicted by Eq. (7) ( $c = 1.10$ ), with the difference attributed to the imperfections of the IBURP pulses.

There are 12 Gly residues in the HIV-1 protease, with 4 of them located in the flexible flap region and several others also showing rather divergent  $\phi$  angles in the X-ray structures. For most residues in the well ordered parts of the protein, the predicted  $I_B/I_A$  ratios differ somewhat more from unity than observed experimentally

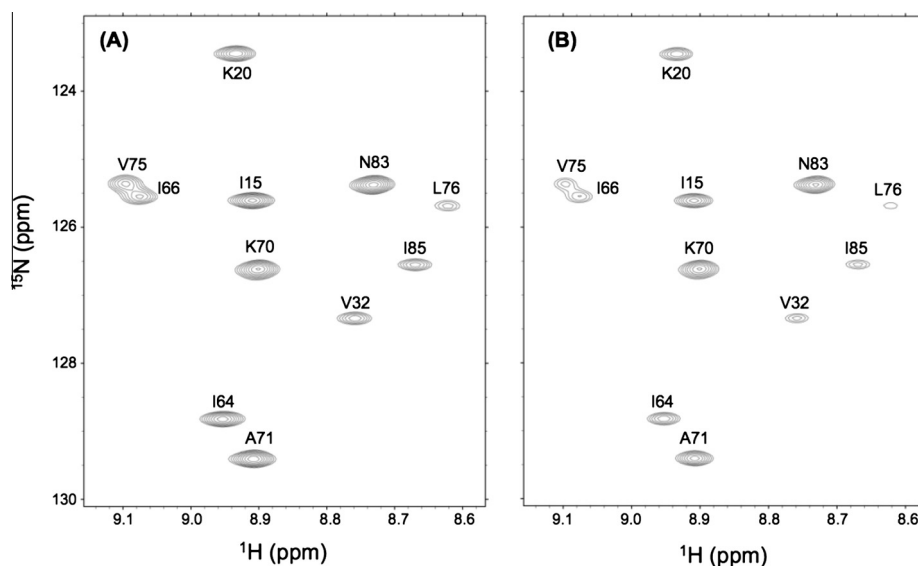


**Fig. 7.** Expanded small region of the reference (A) and attenuated (B)  $^1\text{H}^{\text{N}}\text{-}^{15}\text{N}$  ARTSY-J spectra of HIV-1 protease, recorded at 900 MHz (150  $\mu\text{M}$  dimer concentration; pH 5.7; 298 K). The spectra result from an interleaved acquisition of  $2 \times 350^\circ \times 1280^\circ$  data matrices, for a total measurement time of 17 h. The average S/N in the reference spectrum is ca 120:1.

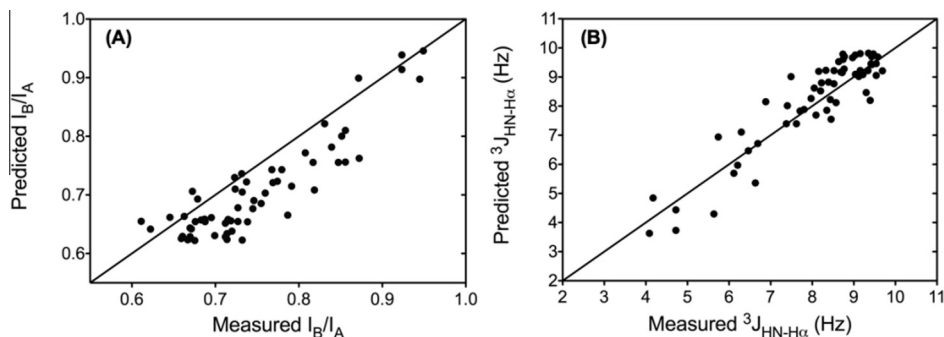


**Fig. 8.** Measurement of  $J_{\text{HNH}\alpha}$  values for HIV-1 protease. (A) Plot of the predicted  $I_B/I_A$  ratios,  $\cos(\pi J_{\text{HNH}\alpha} \tau_d)$ , for 68 non-Gly/Pro residues, against ratios measured with ARTSY-J (900 MHz;  $\tau_d = 30$  ms). (B) Comparison of the experimentally derived  $J_{\text{HNH}\alpha}$  values, after scaling by a factor 1.13, with those predicted by RDC-refined X-ray structures, using the same Karplus parameters as for Fig. 5. Values for  $\theta$ , used in the Karplus equation, correspond to the average taken over the two chains of six high-resolution ( $\leq 1.3 \text{ \AA}$ ) X-ray structures (PDB entries 2IDW, 2NMZ, 2NNK, 2NNP, 3BVA, 3BVB), for which the  $\text{H}^{\text{N}}$  positions were refined by using previously reported RDCs [45]. The rmsd between observed and Karplus-predicted values is 0.64 Hz.

(blue symbols in Fig. 4B), but nevertheless these ratios are directly useful in restricting the possible range of  $\phi$  angles. For example, ratios close to unity, observed for G73 and G78, are consistent with  $\phi$  angles near  $180^\circ$  for these two residues, seen in the X-ray structures.

#### 4. Concluding remarks

Although there are numerous methods available for the measurement of  $^3J_{\text{HNH}\alpha}$ , each of these has its own advantages and disadvantages. The effect of  $^1\text{H}$ – $^1\text{H}$  cross relaxation is manifest in all of these methods, but greatly attenuated in the multiple quantum method of Rexroth and Griesinger [14]. However, this latter method requires a three-dimensional spectrum that records zero- and double-quantum frequencies and involves  $^{13}\text{C}\alpha$  evolution, which has adverse sensitivity consequences for all but the smallest proteins [5]. Our ARTSY-J method is sensitive to  $^1\text{H}$ – $^1\text{H}$  cross relaxation but its impact can be kept small by using a relatively short duration for the  $J$ -dephasing time,  $\tau_d$ . Remarkably, while in direct measurements of  $^3J_{\text{HNH}\alpha}$  from a 1D  $^1\text{H}$  NMR spectrum the effect of cross relaxation on the measured splittings scales very nonlinearly with the size of the coupling, with the effects being largest for small couplings, ARTSY-J yields a linear down scaling by a modest, nearly uniform factor. In practice, we find  $\tau_d \approx 30$  ms to be a reasonable compromise between optimal sensitivity of the method and minimizing the effect of cross-relaxation, resulting in a down-scaling of the apparent coupling by not more than *ca* 10% for a protein with a rotational correlation time of  $\sim 10$  ns. The statistical uncertainty in the extracted  $^3J_{\text{HNH}\alpha}$  scales approximately inversely with the size of the coupling, and for this  $\tau_d$  value a S/N of 50:1 in the reference spectrum corresponds to a random error of only 0.3 Hz for a 10 Hz  $^3J_{\text{HNH}\alpha}$  coupling.

Although the systematic underestimate that can result from pulse miscalibration or radiofrequency field inhomogeneity also leads to a systematic underestimate of the measured  $J$  values, when testing this effect for the small GB3 protein on three different spectrometers, ranging in frequency from 600 to 900 MHz, it was found to be very small ( $\leq 3\%$ ). Both this protein-size-independent error, and the protein-size-dependent cross relaxation induced error, scale approximately linearly with the size of  $^3J_{\text{HNH}\alpha}$ . For HIV protease ( $\tau_c \approx 11$  ns), the combined effects resulted in an underestimate of 12% of the true  $^3J_{\text{HNH}\alpha}$  coupling, as judged by comparison with values predicted on the basis of RDC-refined X-ray structures and previously parameterized Karplus curves.

The convenience, good sensitivity, and high resolution offered by simply obtaining the coupling from two interleaved 2D TROSY-HSQC spectra makes the ARTSY-J method an attractive alternative for measurement of the  $^3J_{\text{HNH}\alpha}$  coupling in  $^{15}\text{N}$ -enriched proteins. We note that the method is not directly suitable for measurement of  $^1\text{H}^{\text{N}}$ – $^1\text{H}$  RDCs in weakly aligned proteins, because the intensity modulation during the  $\tau_d$  dephasing delay corresponds to the product of all couplings to the amide proton from which separate couplings cannot reliably be isolated. E.COSY or quantitative  $J$ -correlation experiments that permit separation of the many couplings to any given proton are more suitable for such studies [8,9,46].

#### Acknowledgments

We thank John Louis for preparing the protease sample, and Fang Li for the GB3 sample. This work was supported by the Intramural Research Program of the National Institute of Diabetes and Digestive and Kidney Diseases and the Intramural Antiviral Target Program of the Office of the Director, NIH.

#### Appendix A. Supplementary material

Supplementary data associated with this article can be found, in the online version, at <http://dx.doi.org/10.1016/j.jmr.2016.05.001>.

#### References

- [1] V.F. Bystrov, Spin-spin couplings and the conformational states of peptide systems, *Prog. NMR Spectrosc.* 10 (1976) 41–81.
- [2] A. Pardi, M. Billeter, K. Wüthrich, Calibration of the angular dependence of the amide proton–C $\alpha$  proton coupling constants,  $^3J_{\text{HNH}\alpha}$ , in a globular protein: use of  $^3J_{\text{HNH}\alpha}$  for identification of helical secondary structure, *J. Mol. Biol.* 180 (1984) 741–751.
- [3] S. Ludvigsen, K.V. Andersen, F.M. Poulsen, Accurate measurements of coupling-constants from 2-dimensional NMR spectra of proteins and determination of phi-angles, *J. Mol. Biol.* 217 (1991) 731–736.
- [4] G.W. Vuister, A. Bax, Quantitative  $J$  correlation: a new approach for measuring homonuclear three-bond ( $^1\text{H}^{\text{N}}$ ) coupling constants in  $^{15}\text{N}$ -enriched proteins, *J. Am. Chem. Soc.* 115 (1993) 7772–7777.
- [5] B. Vogeli, J.F. Ying, A. Grishaev, A. Bax, Limits on variations in protein backbone dynamics from precise measurements of scalar couplings, *J. Am. Chem. Soc.* 129 (2007) 9377–9385.
- [6] A.S. Maltsev, A. Grishaev, J. Roche, M. Zaslhoff, A. Bax, Improved cross validation of a static ubiquitin structure derived from high precision residual dipolar couplings measured in a drug-based liquid crystalline phase, *J. Am. Chem. Soc.* 136 (2014) 3752–3755.
- [7] F. Li, J.H. Lee, A. Grishaev, J. Ying, A. Bax, High accuracy of Karplus equations for relating three-bond  $J$  couplings to protein backbone torsion angles, *ChemPhysChem* 16 (2015) 572–578.
- [8] C. Griesinger, O.W. Sørensen, R.R. Ernst, Practical aspects of the E.COSY technique. Measurement of scalar spin-spin coupling constants in peptides, *J. Magn. Reson.* 75 (1987) 474–492.
- [9] G.T. Montelione, G. Wagner, Accurate measurements of homonuclear H–N–H–alpha coupling-constants in polypeptides using heteronuclear 2D NMR experiments, *J. Am. Chem. Soc.* 111 (1989) 5474–5475.
- [10] A.C. Wang, A. Bax, Determination of the backbone dihedral angles phi in human ubiquitin from reparameterized empirical Karplus equations, *J. Am. Chem. Soc.* 118 (1996) 2483–2494.
- [11] W.P. Aue, J. Karhan, R.R. Ernst, Homonuclear broadband decoupling and two-dimensional  $J$ -resolved spectroscopy, *J. Chem. Phys.* 64 (1976) 4226–4227.
- [12] L.E. Kay, A. Bax, New methods for the measurement of N–C–alpha–H coupling-constants in N-15-labeled proteins, *J. Magn. Reson.* 86 (1990) 110–126.
- [13] C. Lendel, P. Damberg, 3D  $J$ -resolved NMR spectroscopy for unstructured polypeptides: fast measurement of  $^3J(\text{HNH}\alpha)$  coupling constants with outstanding spectral resolution, *J. Biomol. NMR* 44 (2009) 35–42.
- [14] A. Rexroth, P. Schmidt, S. Szalma, T. Geppert, H. Schwalbe, C. Griesinger, New principle for the determination of coupling-constants that largely suppresses differential relaxation effects, *J. Am. Chem. Soc.* 117 (1995) 10389–10390.
- [15] K. Pervushin, R. Riek, G. Wider, K. Wüthrich, Attenuated T-2 relaxation by mutual cancellation of dipole-dipole coupling and chemical shift anisotropy indicates an avenue to NMR structures of very large biological macromolecules in solution, *Proc. Natl. Acad. Sci. USA* 94 (1997) 12366–12371.
- [16] J. Roche, J. Ying, A. Bax, Accurate measurement of  $^3J_{\text{HNH}\alpha}$  couplings in small or disordered proteins from WATERGATE-optimized TROSY spectra, *J. Biomol. NMR* 64 (2016) 1–7.
- [17] F. Lohr, J.M. Schmidt, H. Ruterjans, Simultaneous measurement of  $^3J(\text{HN}, \text{H}\alpha)$  and  $^3J(\text{H}\alpha, \text{H}\beta)$  coupling constants in C-13, N-15-labeled proteins, *J. Am. Chem. Soc.* 121 (1999) 11821–11826.
- [18] M. Billeter, D. Neri, G. Otting, Y.Q. Qian, K. Wüthrich, Precise vicinal coupling-constants  $^3J(\text{HN-HA})$  in proteins from nonlinear fits of  $J$ -modulated  $^{15}\text{N}, ^1\text{H}$ -COSY experiments, *J. Biomol. NMR* 2 (1992) 257–274.
- [19] H. Kuboniwa, S. Grzesiek, F. Delaglio, A. Bax, Measurement of HN–H $\alpha$   $J$  couplings in calcium-free calmodulin using new 2D and 3D water-flip-back methods, *J. Biomol. NMR* 4 (1994) 871–878.
- [20] D. Sitkoff, D.A. Case, Theories of chemical shift anisotropies in proteins and nucleic acids, *Prog. Nucl. Magn. Reson. Spectrosc.* 32 (1998) 165–190.
- [21] Y. Shen, A. Bax, SPARTA plus: a modest improvement in empirical NMR chemical shift prediction by means of an artificial neural network, *J. Biomol. NMR* 48 (2010) 13–22.
- [22] J.T. Nielsen, H.R. Eghbalian, N.C. Nielsen, Chemical shift prediction for protein structure calculation and quality assessment using an optimally parameterized force field, *Prog. Nucl. Magn. Reson. Spectrosc.* 60 (2012) 1–28.
- [23] F. Delaglio, S. Grzesiek, G.W. Vuister, G. Zhu, J. Pfeifer, A. Bax, NMRpipe – a multidimensional spectral processing system based on Unix pipes, *J. Biomol. NMR* 6 (1995) 277–293.
- [24] N.C. Fitzkee, A. Bax, Facile measurement of H-1-N-15 residual dipolar couplings in larger perdeuterated proteins, *J. Biomol. NMR* 48 (2010) 65–70.
- [25] K.V. Pervushin, G. Wider, K. Wüthrich, Single transition-to-single transition polarization transfer (ST2-PT) in  $^{15}\text{N}, ^1\text{H}$ -TROSY, *J. Biomol. NMR* 12 (1998) 345–348.
- [26] T. Schulte-Herbruggen, O.W. Sørensen, Clean TROSY: compensation for relaxation-induced artifacts, *J. Magn. Reson.* 144 (2000) 123–128.

- [27] H. Geen, R. Freeman, Band-selective radiofrequency pulses, *J. Magn. Reson.* 93 (1991) 93–141.
- [28] L.E. Kay, P. Keifer, T. Saarinen, Pure absorption gradient enhanced heteronuclear single quantum correlation spectroscopy with improved sensitivity, *J. Am. Chem. Soc.* 114 (1992) 10663–10665.
- [29] R. Bruschweiler, C. Griesinger, O.W. Sørensen, R.R. Ernst, Combined use of hard and soft pulses for omega-1 decoupling in two-dimensional NMR spectroscopy, *J. Magn. Reson.* 78 (1988) 178–185.
- [30] G.S. Harbison, Interference between J-couplings and cross-relaxation in solution NMR-spectroscopy – consequences for macromolecular structure determination, *J. Am. Chem. Soc.* 115 (1993) 3026–3027.
- [31] R. Freeman, S.P. Kempell, M.H. Levitt, Radiofrequency pulse sequences which compensate their own imperfections, *J. Magn. Reson.* 38 (1980) 453–479.
- [32] M. Goldman, Interference effects in the relaxation of a pair of unlike spin-1/2 nuclei, *J. Magn. Reson.* 60 (1984) 437–452.
- [33] J. Cavanagh, W.J. Fairbrother, A.G. Palmer, M. Rance, N. Skelton, *Protein NMR Spectroscopy: Principles and Practice*, Elsevier Academic Press, Burlington, MA, 2007. eq 5.15.
- [34] E.D. Becker, *High Resolution NMR*, third ed., Theory and Applications, Academic Press, San Diego, 2000, pp. 165–168.
- [35] J.B. Hall, D. Fushman, Characterization of the overall and local dynamics of a protein with intermediate rotational anisotropy: differentiating between conformational exchange and anisotropic diffusion in the B3 domain of protein G, *J. Biomol. NMR* 27 (2003) 261–275.
- [36] L. Yao, B. Vogeli, D.A. Torchia, A. Bax, Simultaneous NMR study of protein structure and dynamics using conservative mutagenesis, *J. Phys. Chem. B* 112 (2008) 6045–6056.
- [37] J.P. Derrick, D.B. Wigley, The 3rd IgG-binding domain from streptococcal protein-G – an analysis By X-ray crystallography of the structure alone and in a complex with Fab, *J. Mol. Biol.* 243 (1994) 906–918.
- [38] T.S. Ulmer, B.E. Ramirez, F. Delaglio, A. Bax, Evaluation of backbone proton positions and dynamics in a small protein by liquid crystal NMR spectroscopy, *J. Am. Chem. Soc.* 125 (2003) 9179–9191.
- [39] F. Li, A. Grishaev, J. Ying, A. Bax, Side chain conformational distributions of a small protein derived from model-free analysis of a large set of residual dipolar couplings, *J. Am. Chem. Soc.* 137 (2015) 14798–14811.
- [40] R. Ishima, D.I. Freedberg, Y.X. Wang, J.M. Louis, D.A. Torchia, Flap opening and dimer-interface flexibility in the free and inhibitor-bound HIV protease, and their implications for function, *Struct. Fold. Des.* 7 (1999) 1047–1055.
- [41] R. Ishima, P.T. Wingfield, S.J. Stahl, J.D. Kaufman, D.A. Torchia, Using amide H-1 and N-15 transverse relaxation to detect millisecond time-scale motions in perdeuterated proteins: application to HIV-1 protease, *J. Am. Chem. Soc.* 120 (1998) 10534–10542.
- [42] J.M. Sayer, F. Liu, R. Ishima, I.T. Weber, J.M. Louis, Effect of the active site D25N mutation on the structure, stability, and ligand binding of the mature HIV-1 protease, *J. Biol. Chem.* 283 (2008) 13459–13470.
- [43] N. Tjandra, P. Wingfield, S. Stahl, A. Bax, Anisotropic rotational diffusion of perdeuterated HIV protease from 15N NMR relaxation measurements at two magnetic fields, *J. Biomol. NMR* 8 (1996) 273–284.
- [44] R. Koradi, M. Billeter, K. Wuthrich, MOLMOL: a program for display and analysis of macromolecular structures, *J. Mol. Graph.* 14 (1996) 51–55.
- [45] J. Roche, J.M. Louis, A. Bax, Conformation of inhibitor-free HIV-1 protease derived from NMR spectroscopy in a weakly oriented solution, *ChemBioChem* 16 (2015) 214–218.
- [46] B. Vogeli, L. Yao, A. Bax, Protein backbone motions viewed by intrasidue and sequential H-N-H-alpha residual dipolar couplings, *J. Biomol. NMR* 41 (2008) 17–28.
- [47] M. Piotto, V. Saudek, V. Sklenár, Gradient-tailored excitation for single-quantum NMR spectroscopy of aqueous solutions, *J. Biomol. NMR* 2 (1992) 661–665.